THE ASTROPHYSICAL JOURNAL, 336:843–853, 1989 January 15

X-RAY HALOS AROUND SUPERNOVA REMNANTS

CHRISTOPHER W. MAUCHE
Harvard-Smithsoniân Center for Astrophysics, and Earth and Space Sciences Division, Los Alamos National Laboratory
AND
PAUL GORENSTEIN
Harvard-Smithsonian Center for Astrophysics
Received 1988 March 23; accepted 1988 June 29

ABSTRACT

We report on the results of an *Einstein Observatory* imaging proportional counter investigation of the X-ray halos of the four brightest young Galactic supernova remnants: the Crab Nebula, Cas A, Tycho's, and Kepler's supernova remnant. We find that the size, shape, and rough intensity of each of these sources are consistent with the measured properties of the X-ray halos of compact Galactic X-ray sources, and as such are consistent with an origin due solely to the scattering of X-rays by interstellar grains.

Subject headings: interstellar: grains — nebulae: Crab Nebula — nebulae: supernova remnants — X-rays: sources

I. INTRODUCTION

As a continuation of our study of the effects of the scattering of X-rays by interstellar grains, we have undertaken an observational study of the X-ray halos of the four brightest young Galactic supernova remnants observed with the imaging instruments aboard the *Einstein Observatory*: the Crab Nebula, Cas A, Tycho's, and Kepler's supernova remnant (SNR). Previous papers in this series have dealt with the number density and size distribution of interstellar grains and with the properties of the X-ray halos of compact Galactic X-ray sources (Mauche and Gorenstein 1986, hereafter Paper I), with the effects of the X-ray scattering halo on the observational properties of Cyg X-3 (Molnar and Mauche 1986), and with purported existence of the soft X-ray halo around the dwarf nova SU UMa (Mauche 1987). Armed with the insight gained by these investigations, we consider in the present paper the properties of the X-ray halos of young Galactic supernova remnants.

Previous investigations of the large-scale surface brightness profiles of supernova remnants have offered increasingly convincing evidence of the existence of X-ray halos around these objects. Toor, Palmieri, and Seward (1976) have shown that the characteristics of the extended source of soft X-ray emission apparent in data from a rocket observation of a lunar occultation of the Crab Nebula are consistent with an intrinsic thermal origin in the Crab Nebula's putative blast wave or an X-ray halo formed by the scattering of X-rays by interstellar grains. Subsequently, Charles and Culhane (1977) have reported additional evidence of the existence of this extended emission with the X-ray telescopes aboard the *Copernicus* satellite. More recent observations appear to rule out the possibility that this extended emission is due to a thermal source because of the failure of the focal plane crystal spectrometer aboard the *Einstein Observatory* to detect X-ray emission lines at positions to the north and south of the nebula (Schattenburg *et al.* 1980). In a previous publication (Mauche and Gorenstein 1985*a*), we have argued that the size, shape, and intensity of the extended emission around the Crab Nebula is consistent with that of an X-ray halo formed by the scattering of X-rays by interstellar grains, and have set an upper limit on the thermal X-ray emission from a blast wave of radius 9′ of $\sim 1\%$ of the total 0.5–3.5 keV luminosity of the Crab Nebula. This upper limit is an order of magnitude or more below the luminosity of Cas A, Tycho's, and Kepler's SNR (which are 2–3 times younger than the Crab), but it is still above that of SN 1006.

In addition to these studies of the Crab Nebula, Stewart, Fabian, and Seward (1983) have reported evidence for weak large-scale X-ray emission from Cas A using high-resolution imager data from the *Einstein Observatory*. They note that this emission could be due to intrinsic thermal or nonthermal processes or to the scattering of X-rays by interstellar grains. This halo has been interpreted by Morfill, Drury, and Aschenbach (1984) as evidence of the diffusive shock acceleration of cosmic rays in Cas A. Another possibility for the origin of the extended emission surrounding Cas A raised by Stewart, Fabian, and Seward (1983) lies in the shock-heating of matter ahead of the bulk ejecta in Cas A's blast wave by fast-moving clumped supernova ejecta. This possibility has subsequently received both theoretical support with the consideration by Hamilton (1985) of supernova blast waves driven by clumped ejecta, and observational support with the discovery by Fesen, Becker, and Blair (1987) of fast-moving nitrogen-rich knots of ejecta well outside Cas A's X-ray, optical, and radio shell. Despite the attractiveness of this explanation for the origin of the extended X-ray emission around Cas A, we have argued elsewhere (Mauche and Gorenstein 1985*b*), and will argue below, that the size, shape, and rough intensity of the extended emission around Cas A—and, indeed, around Tycho's and Kepler's SNR—is consistent with that of an X-ray halo formed by the scattering of X-rays by interstellar grains.

The plan of this paper is as follows. In § II we describe our observations, data analysis, and methods of model construction. In § III we compare our measured and model surface brightness profiles to reveal the presence of large-scale extended X-ray emission around the Crab Nebula, Cas A, Tycho's, and Kepler's SNR. In § IV we determine the size, shape, and intensity of the extended emission around each of these supernova remnants and argue that the origin of this emission is due to the scattering of X-rays by interstellar grains. This is followed in § V by a summary of our results.

II. OBSERVATIONS, DATA ANALYSIS, AND MODEL CONSTRUCTION

The Crab Nebula, Cas A, Tycho's, and Kepler's SNR were each observed with the high-resolution imager (HRI) and imaging proportional counter (IPC) instruments aboard the *Einstein Observatory*. (The observatory and its instruments have been described by Giacconi *et al.* 1979.) Previous studies of the data obtained with these instruments on these supernova remnants have been published by Murray *et al.* (1979), Fabian *et al.* (1980), Dickel *et al.* (1982), Reid, Becker, and Long (1982), Seward, Gorenstein, and Tucker (1983), White and Long (1983), and Brinkmann, Aschenbach, and Langmeier (1985). Whereas these studies have concentrated on the detailed structure of these remnants, we instead will concentrate on the large-scale surface brightness profiles of these remnants relating to the existence of their X-ray halos.

As stressed in our earlier study (Paper I), a quantitative analysis of the surface brightness profiles of sources observed by the *Einstein Observatory* with the HRI and IPC requires a clear understanding of the point response function (PRF) of these instruments. However, because calibration data were obtained during testing at Marshall Space Flight Center prior to the observatory's launch, the energy and pulse height channel dependence of the PRF of these instruments is well known. The energy dependence of the PRF of the observatory's imaging-forming mirror elements was determined during testing of the HRI/mirror combination at 10 energies between 0.2 and 4.5 keV. The resulting profiles have prominent energy-dependent power-law wings due to scattering from surface imperfections in the mirror elements. Similarly, the PRF of the IPC was determined during testing of the IPC/mirror combination. In addition to the energy-dependent power-law wings generated by scattering in the mirror, the PRF of the IPC has an energy- and pulse height channel- (hence gain-) dependent Gaussian core due to this instrument's finite spatial resolution. From a detailed study of this calibration data (see Paper I), we have assembled a library of nearly 100 model PRFs to characterize the energy dependence of the PRF of the HRI (10 PRFs) and the energy and pulse height channel dependence of the PRF of the IPC (81 PRFs).

These model PRFs are added together with weights determined by the spectrum of a given source (and, in the case of the IPC, by the gain of the detector during a given observation) to determine the PRF for a given source during a given observation. Rather than determine these weights by attempting to fit the spectra of the Crab Nebula, Cas A, Tycho's, and Kepler's SNR using the pulse height data supplied by the IPC, we have instead drawn from the rich literature on the subject of the spectra of these supernova remnants to determine the correct spectral distributions to fold through the response function of the IPC to determine the weights needed to construct the PRF for each of these sources. For the spectrum of the Crab Nebula, we have used the power-law spectral distribution given by Schattenburg and Canizares (1986); for Cas A we have used the spectral distribution supplied to us by A. Szymkowiak (Szymkowiak 1987); for Tycho's SNR we have used the non-equilibrium reverse-shock model spectrum of Hamilton, Sarazin, and Szymkowiak (1986) supplied to us by A. Hamilton (Hamilton 1987); and for Kepler's SNR we have used the nonequilibrium enhanced-abundance reverse-shock model spectrum of Hughes and Helfand (1985) supplied to us by J. Hughes (Hughes 1986). These spectral distributions are used in the manner described in Paper I to determine the weights used to construct a single PRF for the HRI and IPC for a given source from the library of (*a*) 10 PRFs which describe the energy dependence of the PRF of the HRI and (*b*) 81 PRFs which describe the energy and pulse height channel dependence of the PRF of the IPC.

Given these PRFs, it is a simple matter in the case of point sources (e.g., compact X-ray sources), to compare the PRF to the measured surface brightness profile of a given source to reveal the source's X-ray halo. In the case of extended sources, however, an additional step is required because it is necessary to know the true surface brightness distribution of the source in the absence of the degrading effects of the PRF of the mirror and the scattering of X-rays by interstellar grains. Consequently, the second step in studying the X-ray halos of extended sources involves the construction of a model of the true surface brightness distribution of each source. After convolving this model surface brightness distribution with the spectrum- (and, in the case of the IPC, gain-) dependent PRF of the HRI or IPC, the resulting convolved model surface brightness profile can be compared to the measured surface brightness profile of the source under investigation to reveal the source's X-ray halo.

The construction of these model surface brightness distributions were accomplished in two ways. In the first, we created a mock-up of the effective surface brightness distribution of each source by means of a simple model. In the case of the Crab Nebula, this model takes the form of a Gaussian of width σ; in the case of the shell-type remnants, this model takes the form of a uniform shell of emission with outer radius R and thickness $r = fR$, where $f = 0.15$, 0.20, and 0.25. In the second way models were constructed, we used the surface brightness distribution of a given source measured by the HRI as the model for IPC. Ignoring for the moment the degrading effects of the PRF of the mirror, this procedure is possible because the HRI measures the surface brightness distribution of an extended source with a spatial resolution which is much finer ($\sim 2''$) than the spatial resolution of the IPC ($\sim 60''$). Consequently, to first order, the HRI measures the true surface brightness distribution of an extended source. Conceptually, it should be possible to deconvolve the surface brightness distribution of an extended source measured by the HRI with the PRF of the mirror to obtain the true surface brightness of a given source free of the degrading effects of the scattering of X-rays by surface imperfections in the mirrors. In practice, however, this is not a simple task. Consequently, we have settled with taking as the model for the true surface brightness distribution of each of our sources the surface brightness distribution measured by the HRI interior to a given radius and zero beyond that radius. This procedure removes the power-law wings of the measured surface brightness distribution obviously associated with the scattering of X-rays by surface imperfections in the mirrors while preserving the true surface brightness distribution of a given source interior to the radius at which the image is truncated. This approximation to the true surface brightness distribution suffices if we are not interested in, nor sensitive to, the small-scale structure of the supernova remnant under investigation.

To illustrate this point, consider Figure 1, which shows the surface brightness profile of the Crab Nebula as measured by the HRI. Interior to $\sim 80''$, the angle-averaged surface brightness profile of the nebula is well-approximated by a Gaussian of width of $\sim 28''.5$. Beyond that radius, two orders of magnitude below the peak central surface brightness of the nebula,

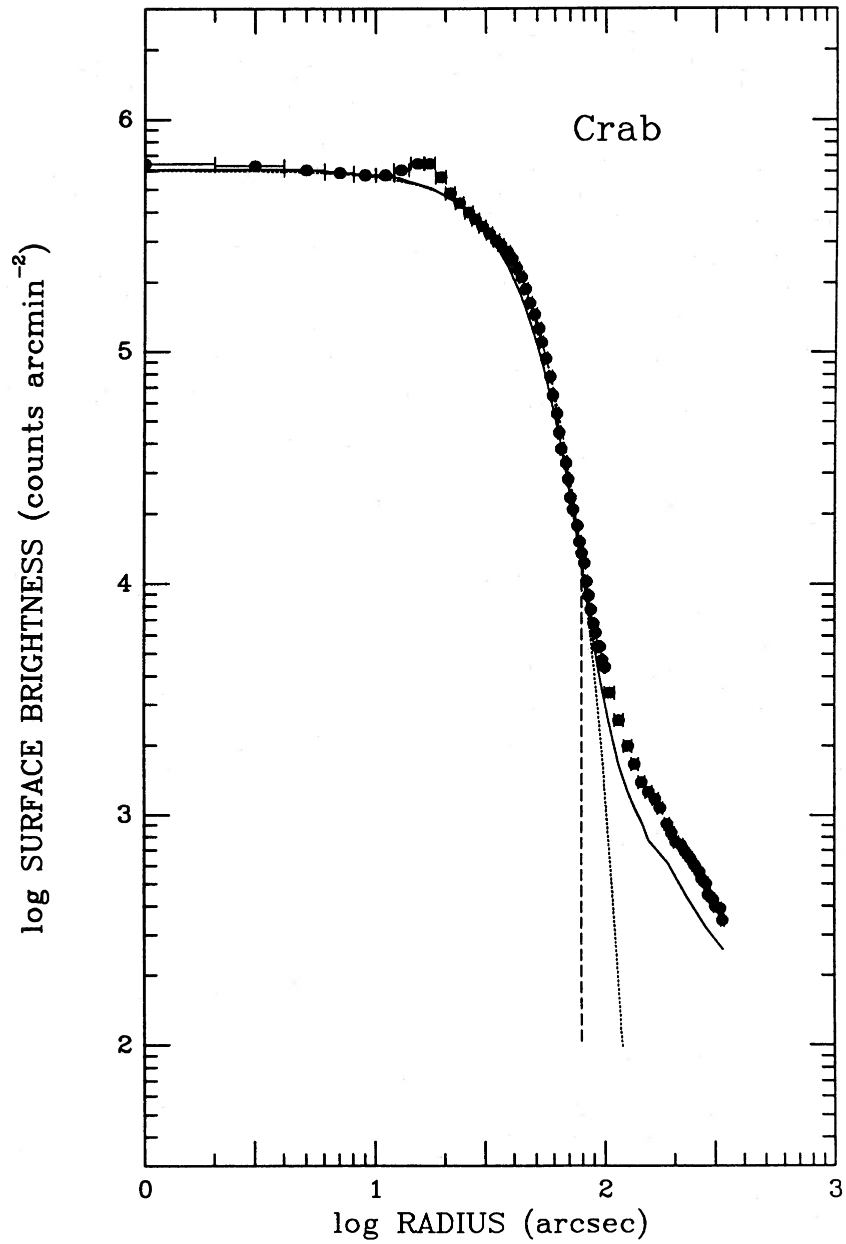

FIG. 1.—The measured and model surface brightness profiles for the HRI image of the Crab Nebula. The measured surface brightness profile is given by the filled circles with error bars; the model surface brightness profile, a Gaussian of width 28″.5, is given by the dotted curve; the surface brightness profile of a Gaussian of width 26″ which has been convolved with the PRF of the mirror at 1.5 keV is given by the solid line. The dashed line indicates the effect on the measured surface brightness profile of truncating the HRI image at 80″.

the surface brightness profile flares out in a manner which is to zeroth order consistent with the PRF of the mirror. We clearly could take as the intrinsic surface brightness distribution of the Crab Nebula either the surface brightness distribution of a Gaussian of width $\sim 28''.5$, or the surface brightness distribution measured by the HRI out to $\sim 80''$ and zero beyond that radius. These possibilities are indicated by the dotted and dashed curves, respectively, in Figure 1. In a similar manner, the surface brightness distribution of the shell-type remnants can be taken either as the surface brightness distribution of a uniform shell of emission with the appropriate dimensions or the surface brightness distribution as measured by the HRI out to some radius and zero beyond. To test the sensitivity of the radius at which the HRI images are truncated, we will in every case produce three different model surface brightness distributions by truncating a given HRI image of a given remnant at three different radii.

Having outlined the procedures we have adopted for dealing with the PRF and with the extended nature of the supernova remnants, we now turn to consider the manner in which the data are handled. Given the HRI and IPC observations of the Crab Nebula, Cas A, Tycho's, and Kepler's SNR, we proceed in the same manner as with the compact X-ray source (see Paper I), and construct radially binned, azimuthally summed surface brightness profiles of the images of these remnants. As before, background has been subtracted by scaling a deep survey field to the same length of time as each of our source observations. In each case, circular symmetry has been assumed, and azimuthal integrations have been performed over all angles.

For completeness, we list in Table 1 the sequence numbers of the observations used in this analysis. We note that sequence 10369 does not appear in the *Einstein Observatory Catalog of Observations* (Seward and Martenis 1986) because it was mistakenly merged with sequence 10370, which is an observation of the Crab Nebula by the IPC with the aluminum filter in place. We have extracted sequence 10369 from sequence 10370 by separating the former sequence from the latter at the point the aluminum filter was brought into place. In the following section, we will consider in more detail the HRI and IPC images of the Crab Nebula, Cas A, Tycho's, and Kepler's SNR.

III. MEASURED AND MODEL SURFACE BRIGHTNESS PROFILES

A quantitative display of the HRI image of the Crab Nebula is shown in Figure 1. Since we have assumed circular symmetry, the radial binning is centered (roughly 16″ northwest of the pulsar) at the centroid of light in the phase-averaged image. As noted above, interior to ~80″, the angle-averaged surface brightness profile of the nebula is well-approximated by a Gaussian of width of ~28″.5. Beyond that radius, the surface brightness profile flares out in a manner which is at least to zeroth order consistent with the PRF of the mirror. As a semi-quantitative assessment of the effect of the PRF of the mirror on the Crab Nebula's true surface brightness profile, we convolved a two-dimensional Gaussian model of the nebula with the PRF of the mirror at 1.5 keV (the mean energy of the Crab Nebula in the HRI is ~1.1 keV). The resulting surface brightness profile of the convolved model is shown as a continuous curve in Figure 1. As is evident in that figure, the measured surface brightness profile of the Crab Nebula beyond ~100″ is a factor of ~1.5 brighter than the convolved model surface brightness profile. The excess emission beyond ~100″ constitutes the Crab Nebula's X-ray halo.

In order to follow the surface brightness profile of the Crab Nebula beyond the ~6′ available in the off-axis HRI image of this supernova remnant, we show in Figure 2 the surface brightness profile measured from the on-axis IPC image of the Crab Nebula. The power-law wing evident in Figure 1 continues in the IPC image out to at least 30′. In order to investigate whether or not this measured surface brightness profile is consistent with the PRF of the IPC, we constructed models of the Crab Nebula using (*a*) a two-dimensional Gaussian of width 26″, 28″.5, and 31″ and (*b*) the HRI image of the nebula truncated at 50″, 75″, and 100″. These models were convolved with the PRF appropriate to the spectrum of the Crab Nebula and the gain of the detector at the time of the observation. The surface brightness profiles of the resulting convolved HRI models normalized to the measured number of counts within 120″ are shown as the upper dotted curves in Figure 2. The corresponding curves for the convolved Gaussian models are essentially the same as the HRI models and have been omitted from this figure for the sake of clarity. Just as in Figure 1, the measured surface brightness profile of the Crab Nebula is a factor of ~1.5 brighter than the convolved model surface brightness profile. The difference between these profiles reveals the size, shape, and intensity of the large-scale extended emission around this supernova remnant.

In order to investigate the large-scale surface brightness profiles of Cas A, Tycho's, and Kepler's SNR, we proceeded in a similar manner to the one described above and constructed models of these supernova remnants using (*a*) a model of a uniform shell of emission projected onto the plane of the sky with outer radius R and thickness $r = fR$, where $f = 0.15$, 0.20, and 0.25 and (*b*) the HRI images of these remnants truncated at various radii. For Cas A we took $R = 120''$ and truncation radii of 150″, 175″, and 200″; for Tycho's SNR we took $R = 215''$ and truncation radii of 250″, 275″, and 300″; and for Kepler's SNR we took $R = 80''$ and truncation radii of 100″, 115″, and 130″. These models were convolved with the PRF appropriate to the spectrum of the given source and gain of the detector at the time of each observation. The surface brightness profiles of the resulting convolved HRI models normalized to the measured number of counts within 180″, 270″, and 150″ for Cas A, Tycho's, and Kepler's SNR, respectively, are shown as the upper dotted curves in Figures 3–5. The corresponding curves for the convolved uniform-shell models do a poor job of matching the detailed surface brightness profile of each remnant interior to a few shell radii, but beyond that are essentially the same as the HRI models and consequently have been omitted from these figures for the sake of clarity. Just as in the previous figures, the measured surface brightness profiles of these remnants lie above the convolved model surface brightness profiles and consequently show evidence for the presence of large-scale extended emission around each of these remnants.

IV. THE SIZE, SHAPE, AND INTENSITY OF THE X-RAY HALOS

In order to determine the size, shape, and rough intensities of the large-scale extended X-ray emission around each of these supernova remnants, all we need do is subtract the model surface brightness profile from the measured surface brightness profile of each remnant. When this is done, as is clear from Figures 2–5 and 6, the shape of the extended X-ray emission around each of these remnants is roughly power law in form over an interval extending from a few remnant radii out to the edge of the IPC at 30′. In this respect, the size and shape of the extended X-ray emission around each of these supernova remnants is consistent with the size and shape of the grain-scattering X-ray halos around the compact Galactic X-ray sources (see Paper I). In order to determine the intensities of these halos, we need a model of the shape of an X-ray halo so that we may extrapolate the surface brightness profile of the halo from large radii where the intensity of the halo is known, to small radii where the intensity of the halo is unknown due to

TABLE 1

SOURCE INFORMATION

Source	Sequence Number	l	b	A_V (mag)	d (kpc)	References
Crab	I10369, H717	185	−5.8	1.6 ± 0.1	1.9 ± 0.1	1, 2
Cas A	I712, H713	112	−2.1	5 ± 1	2.6	3, 4
Tycho	I2147, H714	120	+1.4	2.3 ± 0.3	$2.2^{+1.5}_{-0.6}$	5
Kepler	I2169, H10295	5	+6.8	$3.5^{+0.1}_{-0.3}$	3.2 ± 0.7	6

REFERENCES.—(1) Wu 1981; (2) Trimble 1973; (3) Troland, Crutcher, and Heiles 1985; (4) Haung and Thaddeus 1985; (5) Albinson *et al.* 1986; (6) Danziger and Goss 1980.

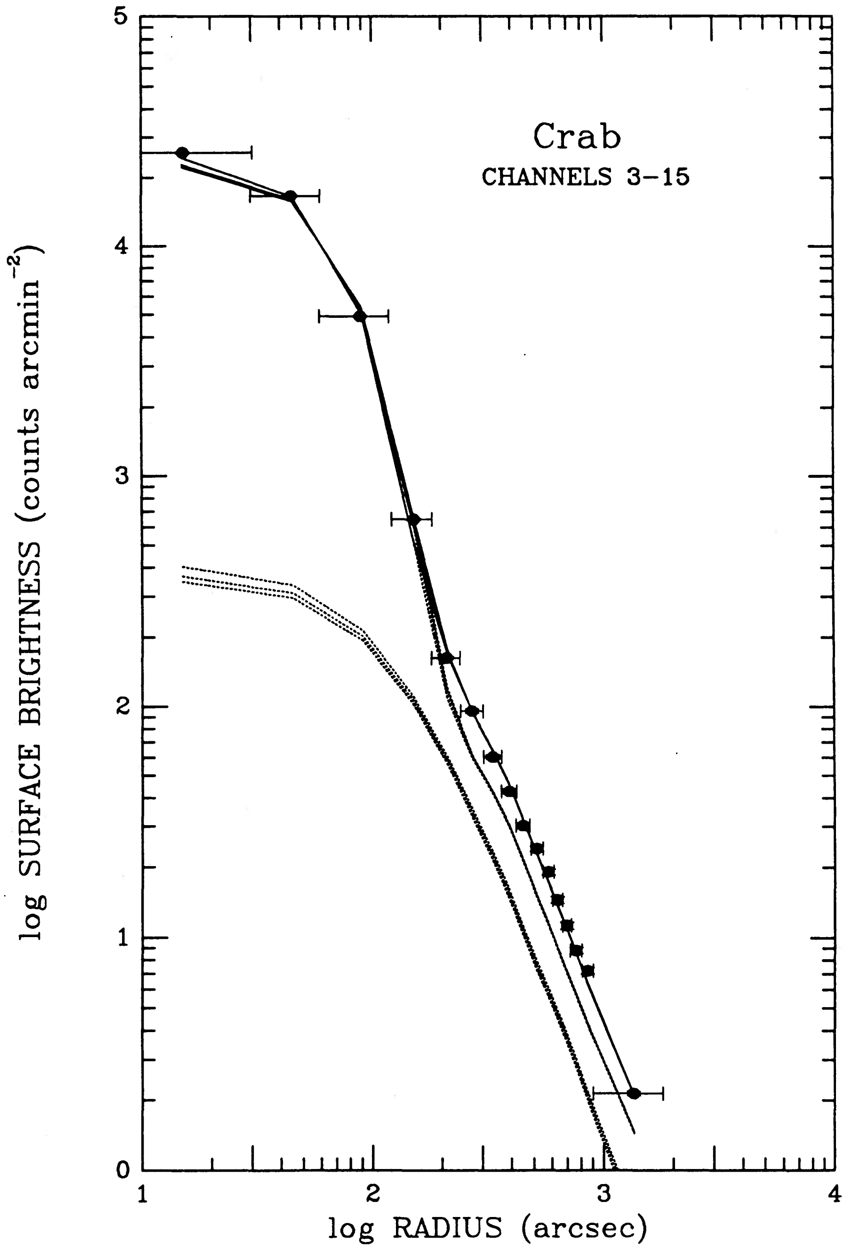

FIG. 2

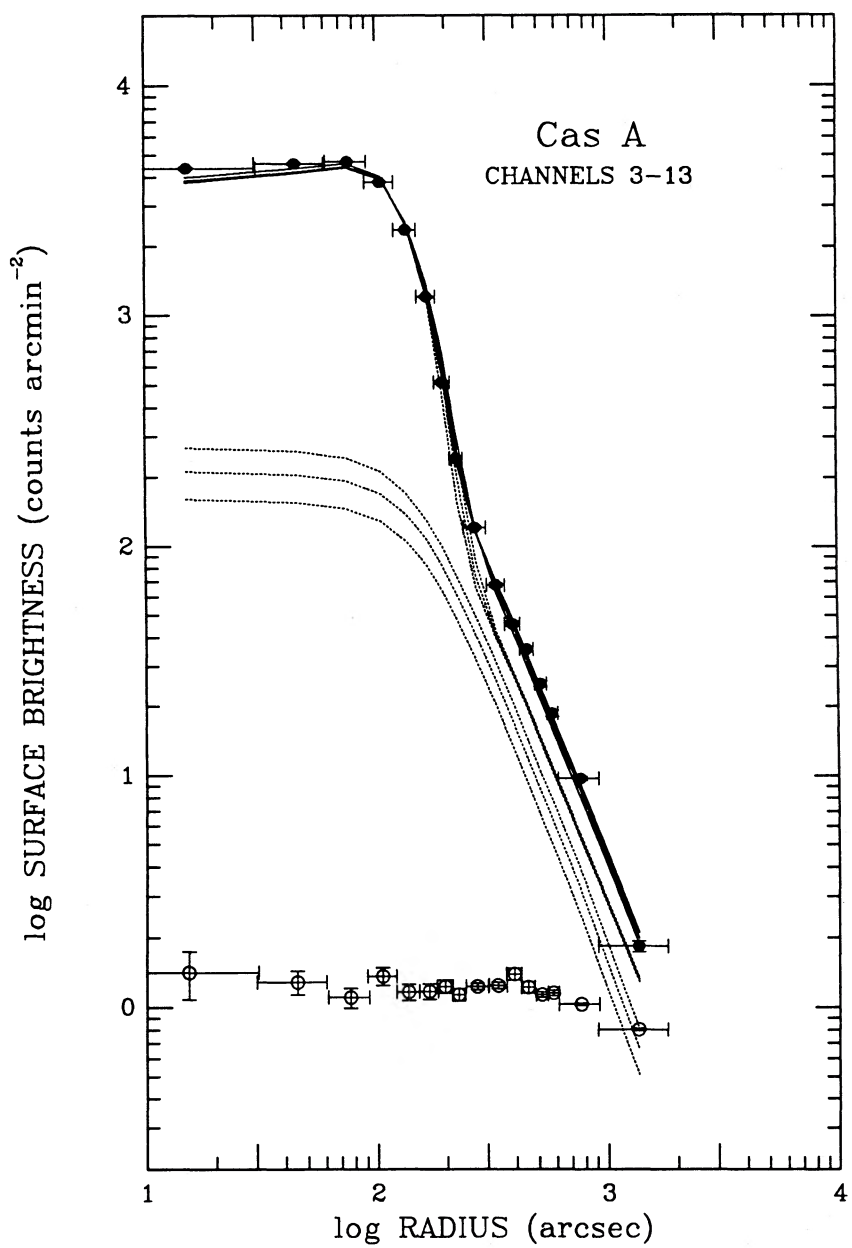

FIG. 3

FIG. 2.—The measured and model surface brightness profile for the IPC image of the Crab Nebula. The measured surface brightness profile is given by the filled circles with error bars; the surface brightness profiles of the convolved HRI models by the upper dotted curves; the surface brightness profiles of the convolved model X-ray halos by the lower dotted curves; and the sum of these model surface brightness profiles at large radii by the solid curves.

FIG. 3.—Similar to Fig. 2, for Cas A. The level of the background is indicated by open circles with error bars.

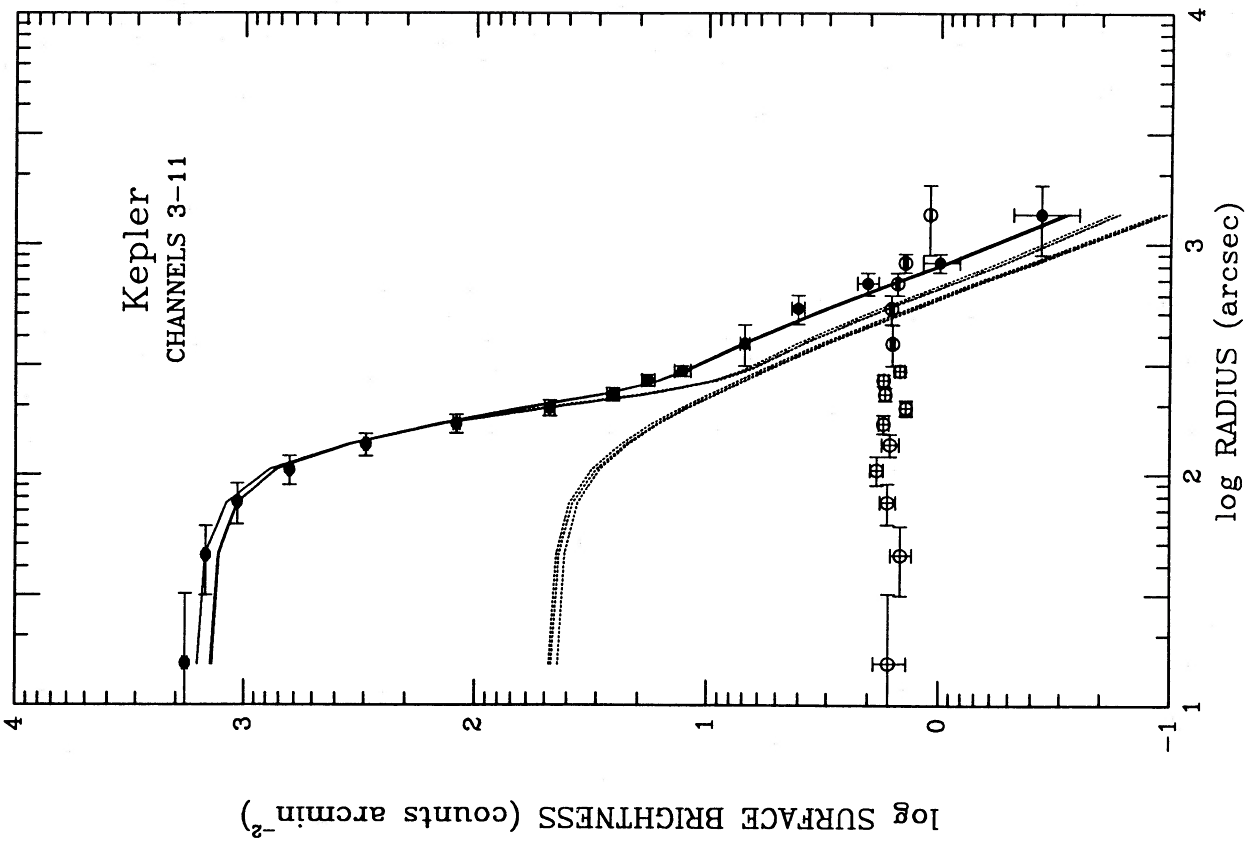

FIG. 5.—Similar to Figs. 2 and 3, for Kepler's SNR

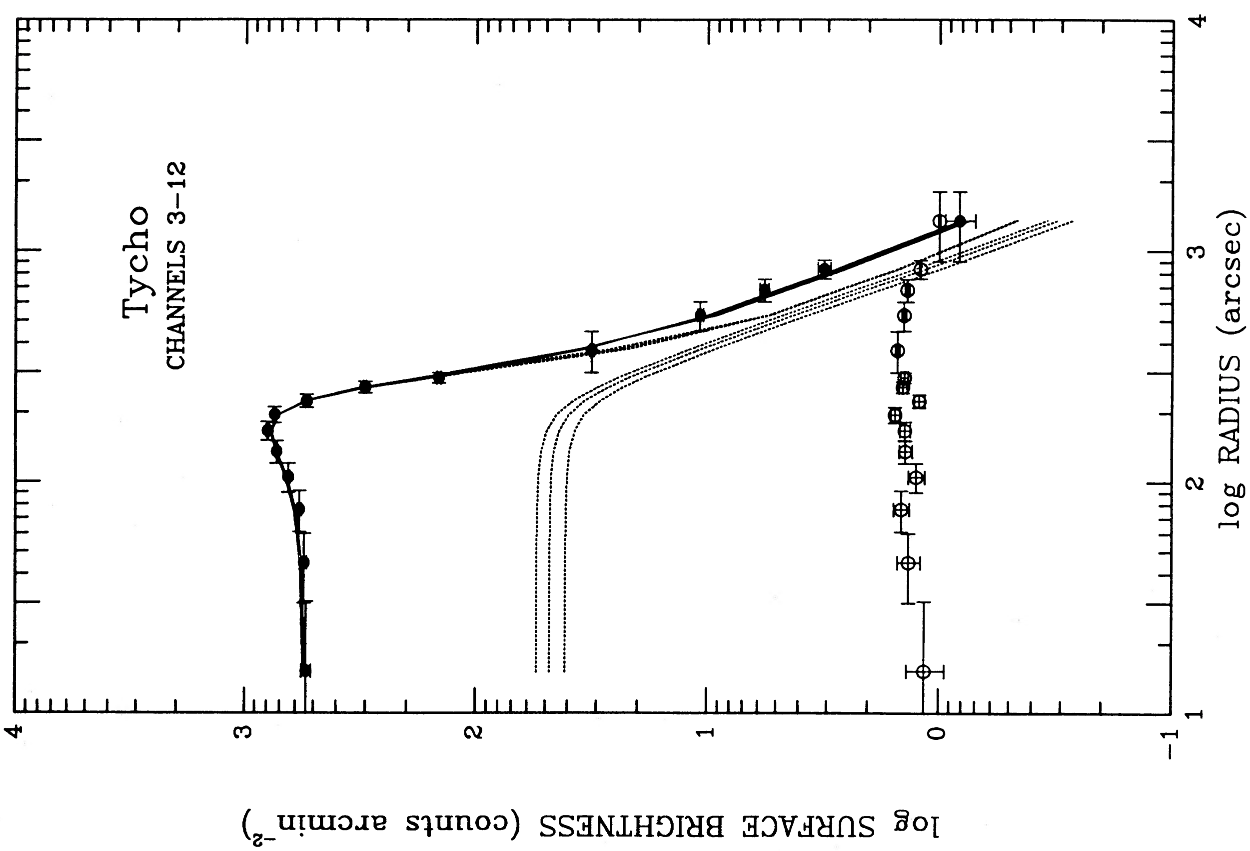

FIG. 4.—Similar to Figs. 2 and 3, for Tycho's SNR

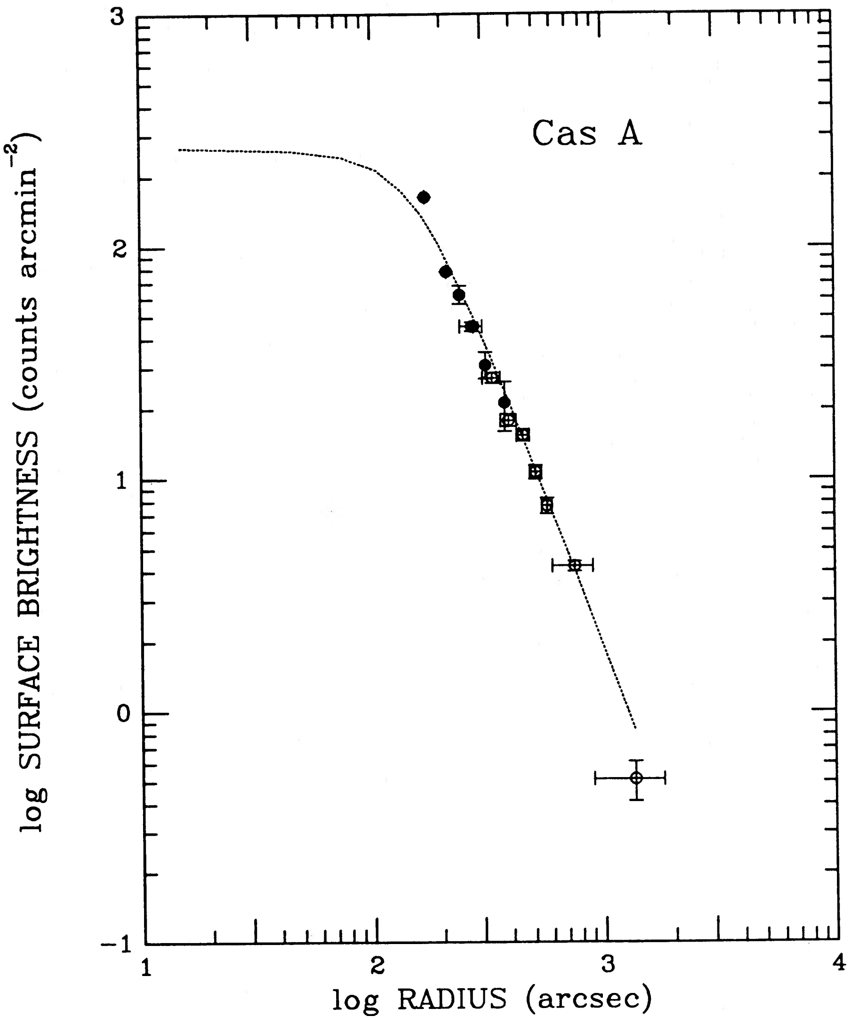

FIG. 6.—The X-ray halo of Cas A. The points for the IPC (*open circles*) are from the difference between the measured and model surface brightness profiles in Fig. 3; the HRI points (*filled circles*) are from Fig. 2 of Stewart, Fabian, and Seward (1983) (with arbitrary normalization) and are from the difference between the measured and model surface brightness profiles in their Fig. 1.

the greater surface brightness of the remnant under investigation. Rather than attempt to determine the shape of the X-ray halos of each of these remnants by means of the type of model-fitting performed in Paper I, we have instead taken as the X-ray halo of a point source the X-ray halo of GX 13+1 as measured by Catura (1983) and Mauche and Gorenstein (1986) (see Fig. 11 of Paper I). Given this model of the shape of the X-ray halo of a point source, we can convolve this model with the extended surface brightness distribution of each supernova remnant to determine the shape of the X-ray halo of each remnant. These convolved model X-ray halos, normalized to the difference between the measured and model surface brightness profiles at large radii for each of our supernova remnants, are shown as the lower dotted curves in Figures 2–5. In each case, three curves are shown corresponding to the three HRI models of the true surface brightness distribution of each source. The corresponding curves for the X-ray halos which have been convolved with the uniform-shell models are essentially the same as the ones shown and have consequently been omitted from these figures for the sake of clarity.

The sum of the model supernova remnant surface brightness profiles and model X-ray halo surface brightness profiles are shown in Figures 2–5 as the solid curves. Given that a single free parameter, the intensity of the X-ray halo, has been used to determine the fit of the solid line to the data points, the fit of these curves to the data is remarkably good. To emphasize this point, we show in Figure 6 a model of the X-ray halo of Cas A superposed on the measured surface brightness distribution of the halo of this source determined by subtracting the 175″ model surface brightness distribution of Cas A from the measured surface brightness distribution. By including the corresponding data from the HRI from Figure 2 of Stewart, Fabian, and Seward (1983), due to the much finer spatial resolution of this instrument, we can determine the shape of the X-ray halo of Cas A from the edge of the remnant at $\sim 150''$ to the edge of the field of view of the IPC at $\sim 30'$. Given the excellent fit of the data to the model in this figure and the excellent fit of the data to the models in Figures 2–5, we conclude that the size and shape of the extended X-ray emission around the Crab Nebula, Cas A, Tycho's, and Kepler's SNR are consistent with an origin due solely to the scattering of X-rays by interstellar grains.

Using the fit of these model X-ray halo surface brightness profiles to the model supernova remnant surface brightness profiles in Figures 2–5, the fractional halo intensity (the intensity of the halo relative to the total intensity) of the Crab Nebula, Cas A, Tycho's, and Kepler's SNR in the ~0.5–3.5 keV bandpass of the IPC are measured to be ~11%, 9%, 8%, and 9%, respectively (see Table 2). To determine whether these intensities are consistent with the fractional halo intensities of other sources for which X-ray halos have been measured, we show in Figure 7 a plot similar to Figure 10 of Paper I: a plot of the measured fractional halo intensity against (*a*) the number of magnitudes of visual extinction, (*b*) the distance to each source, and the distance to each source through the Galaxy's dust layer, whch is taken as a disk with half-thickness 100 pc; for sources out of the plane, $d(\mathrm{kpc}) = 0.1/\sin b$, where b is the source's Galactic latitude. In addition to the data found in Tables 1 and 2 for the Crab Nebula, Cas A, Tycho's, and Kepler's SNR, we include in Figure 7 the data points for all the other X-ray sources for which X-ray halos have been measured and for which either distances or reddening values are available: 3C 273, LMC X-1, 4U 1254−69, 4U 1658−48, GX 13+1, and Cyg X-3 from Paper I; Cyg X-1 from Bode *et al.* (1985); and GX 3+1, GX 9+9, and GX 17+2 from Catura (1983) (the distances for GX 3+1 and GX 17+2 are from Ebisuzaki, Hanawa, and Sugimoto 1984, the reddening for GX 9+9, and the distance and reddening for Cyg X-1 are from Bradt and McClintock 1983). In addition, we have included in Figure 7*a* the reddening value of 11 ± 1 mag for GX 13+1 from Garcia (1987) derived on the consistent assumption that the observed $J-K$ color and J, H, K, and L magnitudes of the infrared counterpart of this source result from the reddening of a giant companion. In both of these figures, the values of the fractional halo intensities of Cas A, Tycho's, and Kepler's SNR appear to be reasonably consistent with the relation defined by the compact Galactic X-ray sources. The fractional halo intensity of the Crab Nebula, on the other hand, appears to be approximately twice as large as expected given its distance or reddening.

What could be the cause of this discrepancy? As shown in Paper I, if the interstellar grains responsible for the scattering of X-rays are the same as those responsible for interstellar extinction, the "optical depth" to the scattering of X-rays

$$\tau_x(E, A_V) = \text{constant} \times A_V(\text{mag})\ E(\text{keV})^{-2}\ , \qquad (1)$$

where E(keV) is the energy in keV, A_V(mag) is the number of magnitudes of visual extinction in mag, and the "constant" is equal to

$$0.10\left(\frac{2Z}{M}\right)^2 \left[\frac{F(E)}{Z}\right]^2 \left(\frac{\rho}{3}\right)^2 a(0.1\ \mu\text{m})^2\ , \qquad (2)$$

where Z is the atomic charge of the element of which the grains are composed, M is its mass number, $F(E)$ is the atomic scattering factor, ρ is the mass density of the grains in g cm^{-3}, and $a(0.1\ \mu\text{m})$ is the effective radius of the grains in units of 0.1 μm. To the extent that, averaged over many kiloparsecs, the density, composition, and effective size of interstellar grains are reasonably constant throughout the Galaxy, the "constant" in equation (2) is ~0.10 and the fractional halo intensity

$$\begin{aligned} i_{\text{Halo}}(E, A_V) &= 1 - \exp\left[-\tau_x(E, A_V)\right] \\ &\approx 1 - \exp\left[-0.10 A_V(\text{mag})\ E(\text{keV})^{-2}\right]. \qquad (3) \end{aligned}$$

Because of the strong energy dependence of this quantity and because of the strong correlation between distance or reddening and the column density of interstellar gas (e.g., Bohlin, Savage, and Drake 1978), the magnitude and shape of the correlation of the fractional halo intensity versus distance or reddening will be strongly affected by the tendency for more distant and more highly reddened sources to have higher mean energies than less distant and less highly reddened sources due to photoelectric absorption of X-rays by the intervening column of interstellar gas. Perhaps more to the point, due to variations in the intrinsic spectra of an ensemble of sources at a given distance or with a given reddening value, a plot of the fractional halo intensity versus distance or reddening will inevitably show a scatter about the statistical relationship between these quantities. Consequently, the observation that the fractional halo intensity of the Crab Nebula is approximately twice as large as expected on the basis of the correlation in Figure 7 may be without significance.

To account for the energy dependence inherent in Figure 7 via the energy dependence of the fractional halo intensity, and to determine whether the fractional halo intensities of the Crab Nebula, Cas A, Tycho's, and Kepler's SNR are consistent with our theoretical expectations, we use equation (3) to determine the expected fractional halo intensity of each of these sources given their reddening values A_V, their adopted X-ray spectral distributions $N(E)$, and the effective area of the IPC (Giacconi *et al.* 1979) $A(E)$:

$$i_{\text{Halo}} = \int i_{\text{Halo}}(E, A_V) N(E) A(E) dE \Big/ \int N(E) A(E) dE\ . \qquad (4)$$

Using this expression, the data in Table 1, and the adopted spectral distributions, the expected fractional halo intensities of the X-ray halos of the Crab Nebula, Cas A, Tycho's, and Kepler's SNR are ~10 ± 1%, 19 ± 3%, 21 ± 2%, and 25^{+1}_{-2}%, respectively, where the errors are due solely to the errors in A_V. The fractional halo intensities of Cas A, Tycho's, and Kepler's SNR are predicted to be so much larger than the value for the Crab Nebula because of (1) the large values of A_V for Cas A, Tycho's, and Kepler's SNR and (2) the intense line radiation in the adopted spectral distribution of these supernova remnants compared to the power-law spectral distribution for the Crab Nebula. Given the close agreement between the observational and theoretical values of the fractional halo intensity of the Crab Nebula and the excellent agreement between the observed and predicted size and shape of the extended X-ray emission around the Crab Nebula, it appears that the proper-

TABLE 2

HALO INTENSITIES

Source	Fractional Halo Intensity[a]	τ_x[b]	$\langle E \rangle$[c] (keV)	$\langle E^* \rangle$[d] (keV)	τ_x^*[e]
Crab	$0.114^{+0.005}_{-0.006}$	$0.121^{+0.006}_{-0.007}$	1.61	1.09	$0.144^{+0.007}_{-0.008}$
Cas A	$0.085^{+0.026}_{-0.016}$	$0.089^{+0.029}_{-0.018}$	1.79	1.42	$0.179^{+0.058}_{-0.036}$
Tycho	$0.082^{+0.014}_{-0.009}$	$0.086^{+0.015}_{-0.010}$	1.31	0.87	$0.065^{+0.011}_{-0.008}$
Kepler	$0.093^{+0.003}_{-0.005}$	$0.098^{+0.003}_{-0.006}$	1.31	1.00	$0.098^{+0.003}_{-0.006}$

[a] $i_{\text{Halo}} = I_{\text{Halo}}/(I_{\text{Halo}} + I_{\text{Core}})$.

[b] The "optical" depth $\tau_x = -\ln(1 - \text{fractional halo intensity})$.

[c] $\langle E \rangle = \int E N(E) A(E) dE / \int N(E) A(E) dE$ is the average photon energy, where $N(E)$ is the photon number spectrum and $A(E)$ is the effective area of the IPC.

[d] $\langle E^* \rangle = \int E\, \sigma_{\text{scat}}(E) N(E) A(E) dE / \int \sigma_{\text{scat}}(E) N(E) A(E) dE$ is the average photon energy weighted by the total scattering cross section.

[e] The "optical" depth τ_x evaluated at 1 keV: $\tau_x^* = \tau_x \langle E^* \rangle^2$.

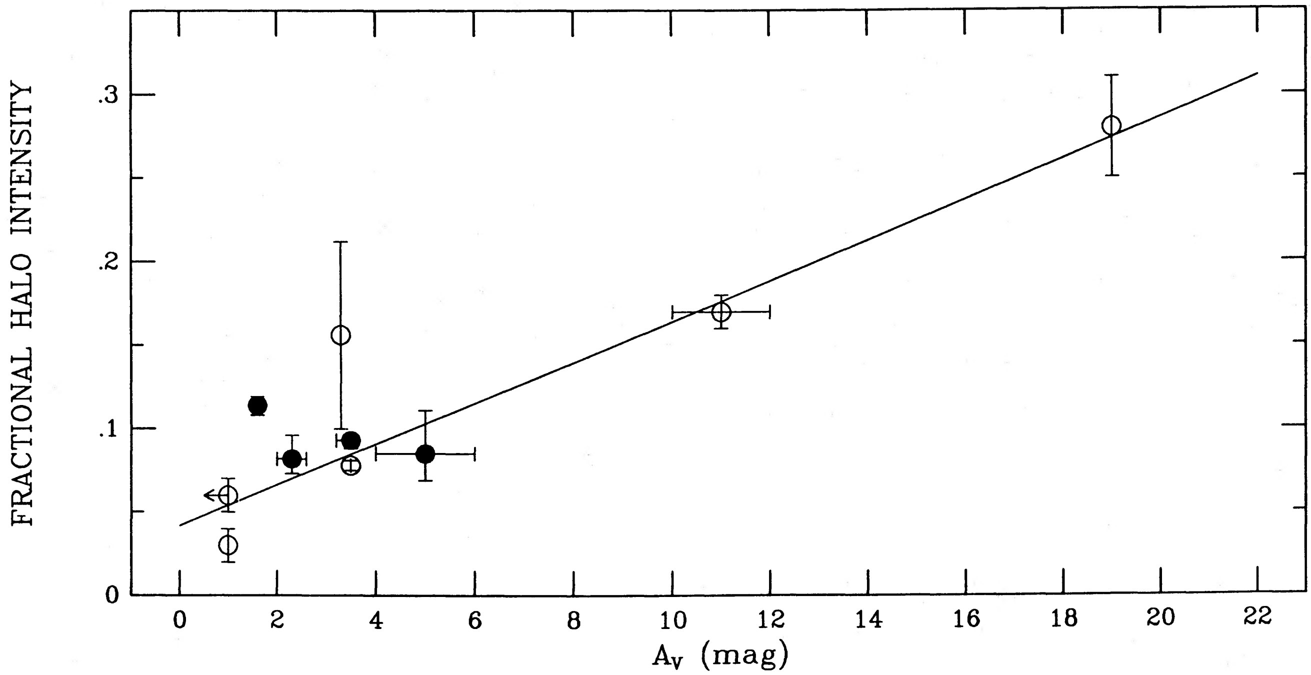

FIG. 7*a*

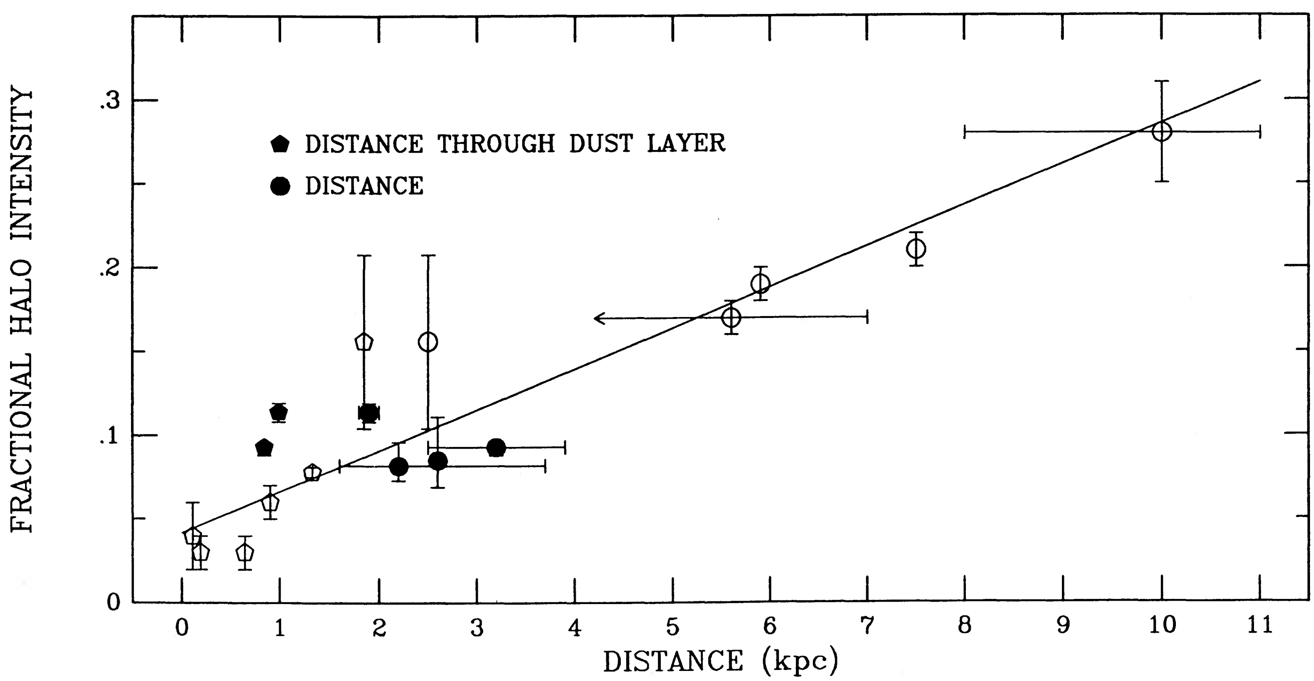

FIG. 7*b*

FIG. 7.—(*a*) The correlation between the fractional halo intensity and the reddening of each source for the data in Tables 1 and 2 (*filled symbols*), Table 2 of Paper I, and additional data due to Catura (1983) and Bode *et al.* (1985) (*open symbols*). The dotted line has been taken from Fig. 10 of Paper I and represents the observed correlation of the compact X-ray sources. (*b*) The correlation between the fractional halo intensity and (1) the distance to each source and (2) the distance to each source through the Galaxy's dust layer for the data in Tables 1 and 2 (*filled symbols*), Table 2 of Paper I, and additional data due to Catura (1983) and Bode *et al.* (1985) (*open symbols*). The dotted line has been taken from Fig. 10 of Paper I and represents the observed correlation of the compact X-ray sources.

ties of the halo of this source are consistent with an origin due solely to the scattering of X-rays by interstellar grains. On the other hand, although the size and shape of the X-ray halos of Cas A, Tycho's, and Kepler's SNR are consistent with an origin due to the scattering of X-rays by interstellar grains, the theoretically predicted intensities of their X-ray halos are approximately twice as large as observed.

What could be the cause of these discrepancies? Possibilities include errors in the form of the adopted spectral distributions, overestimates of the reddening values, an error in the analysis or in the modeling of the data, or real variations in the density, composition, and/or effective size of interstellar grains along the line of sight to Cas A, Tycho's, and Kepler's SNR, and hence to real variations in the value of the "constant" in equation (2). To investigate this latter possibility, we plot in Figure 8 the observationally determined value of this "constant" versus A_V. Specifically, since from equation (2) $\tau_x E(\mathrm{keV})^2/A_V(\mathrm{mag}) = \mathrm{constant} \approx 0.10$, we plot in Figure 8 the quantity $\tau_x{}^*/A_V \equiv \tau_x \langle E^* \rangle^2/A_V$ versus A_V, where

$$\langle E^* \rangle = \int E\sigma_{\mathrm{scat}}(E)N(E)A(E)dE \bigg/ \int \sigma_{\mathrm{scat}}(E)N(E)A(E)dE \quad (5)$$

is the average photon energy weighted by the total scattering cross section, the photon number spectrum, and the effective area of the IPC. Included in Figure 8 are all the sources for which X-ray halos have been measured and for which reddening and $\langle E^* \rangle$ values are available: the Crab Nebula, Cas A, Tycho's SNR, Kepler's SNR, 4U 1254−69, 4U 1658−48, GX 13+1, Cyg X-3, and Cyg X-1. The $\tau_x{}^*$ values in that figure are from Table 2, Table 2 of Paper I, and the information supplied by Bode *et al.* (1985) for Cyg X-1 ($i_{\mathrm{Halo}} \approx 1.3 \times [0.12 \pm 0.04]$, $\langle E^* \rangle = 1.74$ keV is inferred from the quoted spectral information and the effective area of the HRI [Giacconi *et al.* 1979], hence $\tau_x{}^* = 0.515 \pm 0.188$). Furthermore, in addition to the reddening values for the supernova remnants in Table 1, we have adopted reddening values of 1.1 ± 0.2, 2.1, 11 ± 1, 19, and 3.3 ± 0.3 mag for 4U 1254−69, 4U 1658−48, GX 13+1, Cyg X-3, and Cyg X-1, respectively (Motch *et al.* 1987; Motch *et al.* 1985; Garcia 1987; Bradt and McClintock 1983; and Bregman *et al.* 1973 and Wu *et al.* 1982, respectively), where $A_V = 3.2E_{B-V}$ has been used wherever necessary to convert E_{B-V} values to A_V values.

In agreement with our theoretical considerations, Figure 8 demonstrates that the fractional halo intensity of the Crab Nebula is consistent with an origin due to the scattering of X-rays by interstellar grains since this source's measured fractional halo intensity agrees with the theoretical fractional halo intensity given by equation (3) with a constant in equation (1) which ≈ 0.09. Within an uncertainty of $\lesssim 20\%$ in the value of this "constant," the same is apparently true of the fractional halo intensities of GX 13+1, Cyg X-3, and Cyg X-1. On the other hand, the fractional halo intensities of Cas A, Tycho's, and Kepler's SNR are consistent with equation (3) only if the constant in equation (1) ≈ 0.03. The same is apparently true for 4U 1254−69 and 4U 1658−48 if this constant ~ 0.06, although the reddening values for these two point sources are highly uncertain. If this range of values of $\tau_x{}^*/A_V$ represents an intrinsic range of the value of the "constant" in equation (2) due to variations in the density, composition, and/or effective size of interstellar grains along the line of sight to these sources, the measured fractional halo intensities of Cas A, Tycho's, and Kepler's SNR cannot be claimed to be inconsistent with the fractional halo intensities expected from the scattering of X-rays by interstellar grains. On the other hand, if the "constant" in equation (2) $\approx 0.10 \pm$ (say) $\lesssim 20\%$ in all directions on the sky, the measured fractional halo intensities of Cas A, Tycho's, and Kepler's SNR are approximately 2 times smaller than expected on the basis of their adopted spectra

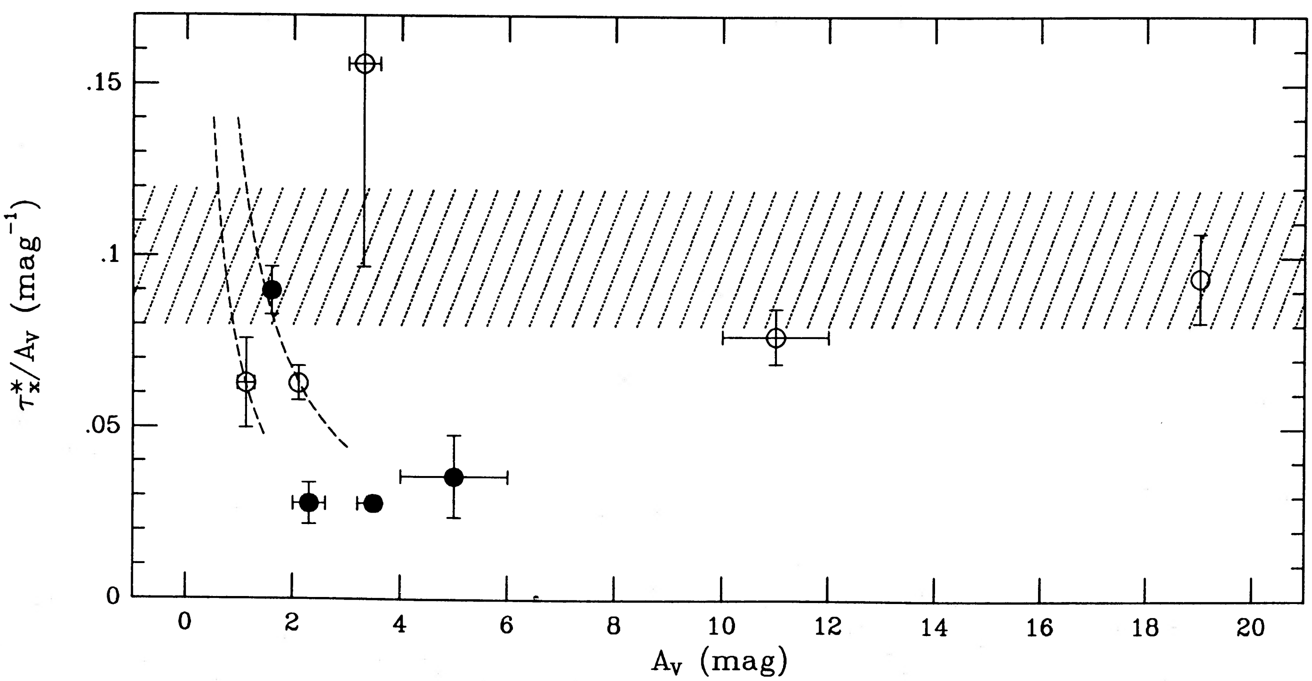

FIG. 8.—Plot of $\tau_x{}^*/A_V$ vs. A_V for the $\tau_x{}^*$ values in Table 2 (*filled symbols*), Table 2 of Paper I, and Bode *et al.* (1985) (*open symbols*) and the A_V values given in the text. The dotted lines delineate the region expected theoretically to include the $\tau_x{}^*/A_V$ values allowed by equation (2). The dashed lines illustrate the paths followed by the data points for 4U 1254−69 and 4U 1658−48 as their adopted A_V values vary.

distributions and reddening values. Alternately, the small value of the "constant" in equation (2) for Cas A, Tycho's, and Kepler's SNR relative to the other sources may be due to a reduction in the effective value of the atomic scattering factor in equation (2) for these sources due to the absorption and anomalous scattering (see, e.g., Martin and Sciama 1970 and Martin 1970) of the emission lines of these emission-line sources by the elements of which interstellar grains are composed.

V. SUMMARY

As noted in the summary in Paper I, the most general result of Catura's (1983), Bode *et al.*'s (1985), and our previous investigations of the X-ray halos formed by the scattering of X-rays by interstellar grains is that these halos are a feature endemic to Galactic X-ray sources. Given this result, it is to be expected that highly reddened Galactic supernova remnants possess X-ray halos due to the scattering of X-rays by interstellar grains. In this paper we have described the procedures necessary to reveal the X-ray halos of extended supernova remnants observed with the imaging instruments aboard the *Einstein Observatory*. In particular, we have described an imaging proportional counter investigation of the X-ray halos of the four brightest young Galactic supernova remnants: the Crab Nebula, Cas A, Tycho's, and Kepler's SNR. We find that the size, shape, and intensity of the X-ray halo of the Crab Nebula are consistent with the measured properties of the X-ray halos of compact Galactic X-ray sources, and as such the X-ray halo of the Crab Nebula is consistent with an origin due solely to the scattering of X-rays by interstellar grains. On the other hand, although the size and shape of the X-ray halos of Cas A, Tycho's, and Kepler's SNR are consistent with an origin due to the scattering of X-rays by interstellar grains, and although the intensities of their X-ray halos are reasonably consistent with the correlation between halo intensity and reddening defined by the compact Galactic X-ray sources, given the adopted spectral distributions and reddening values of these supernova remnants, the intensities of their X-ray halos are consistent with our theoretical expectations (only) if the "constant" in equation (2) ≈ 0.03 rather than the value of ~ 0.09 appropriate to the Crab Nebula and the compact Galactic X-ray sources. Nevertheless, alternate explanations for large-scale X-ray emission previously observed to surround the Crab Nebula (Toor, Palmieri, and Seward 1976; Charles and Culhane 1977) and Cas A (Stewart, Fabian, and Seward 1983) (e.g., the Crab Nebula's putative blast wave [Toor, Palmieri, and Seward 1976], diffusive shock acceleration of cosmic rays in Cas A [Morfill, Drury, and Aschenbach 1984], and shock-heating of matter ahead of the bulk ejecta in Cas A's blast wave by fast-moving clumped supernova ejecta [Stewart, Fabian, and Seward 1983; Hamilton 1985]) are not necessary to account for the observations of these remnants by the *Einstein Observatory*.

The authors are pleased to acknowledge A. Hamilton, J. Hughes, and A. Szymkowiak for generously providing us with X-ray spectra of Tycho's SNR, Kepler's SNR, and Cas A, respectively, D. Fabricant, R. Harnden, and F. Seward for their expert advice concerning subtleties of the IPC, and an anonymous referee for quickly and thoroughly reading and commenting on a preliminary version of this manuscript. This work has been supported by NASA contract NAS8-30751 to the Smithsonian Astrophysical Observatory and by the US Department of Energy.

REFERENCES

Albinson, J. S., Tuffs, R. J., Swinbank, E., and Gull, S. F. 1986, *M.N.R.A.S.*, **219**, 427.
Bode, M. F., Priedhorsky, W. C., Norwell, G. A., and Evans, A. 1985, *Ap. J.*, **299**, 845.
Bohlin, R. C., Savage, B. D., and Drake, J. F. 1978, *Ap. J.*, **224**, 132.
Bradt, H. V. D., and McClintock, J. E. 1983, *Ann. Rev. Astr. Ap.*, **21**, 13.
Bregman, J., Butler, D., Kemper, E., Koski, A., Kraft, R. P., and Stone, R. P. S. 1973, *Ap. J. (Letters)*, **185**, L117.
Brinkmann, W., Aschenbach, B., and Langmeier, A. 1985, *Nature*, **313**, 662.
Catura, R. C. 1983, *Ap. J.*, **275**, 645.
Charles, P. A., and Culhane, J. L. 1977, *Ap. J. (Letters)*, **211**, L23.
Danziger, I. J., and Goss, W. M. 1980, *M.N.R.A.S.*, **190**, 47P.
Dickel, J. R., Murray, S. S., Morris, J., and Wells, D. C. 1982, *Ap. J.*, **257**, 145.
Ebisuzaki, T., Hanawa, T., and Sugimoto, D. 1984, *Pub. Astr. Soc. Japan*, **36**, 551.
Fabian, A. C., Willingale, R., Pye, J. P., Murray, S. S., and Fabbiano, G. 1980, *M.N.R.A.S.*, **193**, 175.
Fesen, R. A., Becker, R. H., and Blair, W. P. 1987, *Ap. J.*, **313**, 378.
Garcia, M. R. 1987, Ph.D. thesis, Harvard University.
Giacconi, R., *et al.* 1979, *Ap. J.*, **230**, 540.
Hamilton, A. J. S. 1985, *Ap. J.*, **291**, 523.
———. 1987, private communication.
Hamilton, A. J. S., Sarazin, C. L., and Szymkowiak, A. E. 1986, *Ap. J.*, **300**, 713.
Haung, Y. L., and Thaddeus, P. 1985, *Ap. J. (Letters)*, **295**, L13.
Hughes, J. P. 1986, private communication.
Hughes, J. P., and Helfand, D. J. 1985, *Ap. J.*, **291**, 544.
Martin, P. G. 1970, *M.N.R.A.S.*, **149**, 221.
Martin, P. G., and Sciama, D. W. 1970, *Ap. Letters*, **5**, 193.
Mauche, C. W. 1987, Ph.D. thesis, Harvard University.
Mauche, C. W., and Gorenstein, P. 1985*a*, in *The Crab Nebula and Related Supernova Remnants*, ed. R. B. C. Henry and M. C. Kafatos (Cambridge: Cambridge University Press), p. 81.
Mauche, C. W., and Gorenstein, P. 1985*b*, *Bull AAS*, **16**, 926.
———. 1986, *Ap. J.*, **302**, 371 (Paper I).
Molnar, L. A., and Mauche, C. W. 1986, *Ap. J.*, **310**, 343.
Morfill, G. E., Drury, L. O'C., and Aschenbach, B. 1984, *Nature*, **311**, 358.
Motch, C., Ilovaisky, S. A., Chevalier, C., and Angebault, P. 1985, *Space Sci Rev.*, **40**, 219.
Motch, C., Pedersen, H., Beuermann, K., Pakull, M. W., and Courvoisier, T. J.-L. 1987, *Ap. J.*, **313**, 792.
Murray, S. S., Fabbiano, G., Fabian, A. C., Epstein, A., and Giacconi, R. 1979, *Ap. J. (Letters)*, **234**, L69.
Reid, P. B., Becker, R. H., and Long, K. S. 1982, *Ap. J.*, **261**, 485.
Schattenburg, M. L., *et al.* 1980, *Ap. J. (Letters)*, **241**, L151.
Schattenburg, M. L., and Canizares, C. R. 1986, *Ap. J.*, **301**, 759.
Seward, F., Gorenstein, P., and Tucker, W. 1983, *Ap. J.*, **266**, 287.
Seward, F. D., and Martenis, P. 1986, *Einstein Observatory Catalog of Observations*, CfA High-Energy Astrophysics report CFA/HEA86-045.
Stewart, G. C., Fabian, A. C., and Seward, F. D. 1983, in *Supernova Remnants and their X-Ray Emission*, ed. J. Danziger and P. Gorenstein (Dordrecht: Reidel), p. 59.
Szymkowiak, A. E. 1987, private communication.
Toor, A., Palmieri, T. M., and Seward, F. D. 1976, *Ap. J.*, **207**, 96.
Trimble, V. 1973, *Pub. A.S.P.*, **85**, 579.
Troland, T. H., Crutcher, R. M., and Heiles, C. 1985, *Ap. J.*, **298**, 808.
White, R. L., and Long, K. S. 1983, *Ap. J.*, **264**, 196.
Wu, C.-C. 1981, *Ap. J.*, **245**, 581.
Wu, C.-C., Eaton, J. A., Holm, A. V., Milgrom, M., and Hammerschlag-Hensberge, G. 1982, *Pub. A.S.P.*, **94**, 149.

PAUL GORENSTEIN: Harvard-Smithsonian Center for Astrophysics, 60 Garden Street, Cambridge, MA 02138

CHRISTOPHER W. MAUCHE: Los Alamos National Laboratory, MS D436, ESS-9, Los Alamos, NM 87545